OPEN ACCESS



Spectroscopic Detection of Alfvénic Waves in the Chromospheric Fibrils of a Solar-quiet Region

Hannah Kwak¹, Jongchul Chae², Eun-Kyung Lim¹, Kyoung-Sun Lee², Donguk Song^{1,3}, and Heesu Yang¹, Korea Astronomy and Space Science Institute, 776 Daedeok-daero, Yuseong-gu, Daejeon 34055, Republic of Korea; hannahk@kasi.re.kr

Astronomy Program, Department of Physics and Astronomy, Seoul National University, 1 Gwanak-ro, Gwanak-gu, Seoul 08826, Republic of Korea

National Astronomical Observatory of Japan, 2-21-1 Osawa, Mitaka, Tokyo 181-8588, Japan

Received 2023 July 10; revised 2023 October 9; accepted 2023 October 23; published 2023 November 20

Abstract

We report the detection of transverse magnetohydrodynamic waves, also known as Alfvénic waves, in the chromospheric fibrils of a solar-quiet region. Unlike previous studies that measured transversal displacements of fibrils in imaging data, we investigate the line-of-sight (LOS) velocity oscillations of the fibrils in spectral data. The observations were carried out with the Fast Imaging Solar Spectrograph of the 1.6 m Goode Solar Telescope at the Big Bear Solar Observatory. By applying spectral inversion to the $H\alpha$ and Ca II 8542 Å line profiles, we determine various physical parameters, including the LOS velocity in the chromosphere of the quiet Sun. In the $H\alpha$ data, we select two adjacent points along the fibrils and analyze the LOS velocities at those points. For the time series of the velocities that show high cross-correlation between the two points and do not exhibit any correlation with intensity, we interpret them as propagating Alfvénic wave packets. We identify a total of 385 Alfvénic wave packets in the quiet-Sun fibrils. The mean values of the period, velocity amplitude, and propagation speed are 7.5 minutes, 1.33 km s⁻¹, and 123 km s⁻¹, respectively. We find that the detected waves are classified into three groups based on their periods, namely, 3, 5, and 10 minute bands. Each group of waves exhibits distinct wave properties, indicating a possible connection to their generation mechanism. Based on our results, we expect that the identification of Alfvénic waves in various regions will provide clues to their origin and the underlying physical processes in the solar atmosphere.

Unified Astronomy Thesaurus concepts: Solar chromosphere (1479); Solar atmosphere (1477); Magnetohydrodynamics (1964); Alfvén waves (23); Quiet Sun (1322)

1. Introduction

The solar chromosphere exhibits a wealth of dynamic finescale structures, which have been revealed in high-resolution observations. These observations have allowed for detailed investigations into the dynamics and physical properties of previously unresolved threadlike structures (Tsiropoula et al. 2012). These structures are referred to by different names, such as mottles, fibrils, dynamic fibrils, and spicules, depending on their locations (on-disk and off-limb), regions (quiet Sun, plage, active region, etc.), and physical properties (e.g., type I and II spicules). These threadlike structures are considered to trace the magnetic field lines (Leenaarts et al. 2012), acting as waveguides for the propagation of magnetohydrodynamic (MHD) waves in the solar atmosphere. Numerous studies have reported the presence of oscillations and waves within these structures (Jess et al. 2015). Transverse motions with periodicity have been observed in mottles (Kuridze et al. 2012, 2013), superpenumbral fibrils (Morton et al. 2021; Chae et al. 2021b, 2022), and spicules (De Pontieu et al. 2007; Jess et al. 2012), indicating the existence of transverse waves propagating along the magnetic field lines within these threadlike structures. These transverse MHD waves are commonly referred to as Alfvénic waves encompassing both Alfvén waves and kink waves, as they share similar characteristics. Alfvénic waves are regarded as a potential

Original content from this work may be used under the terms of the Creative Commons Attribution 4.0 licence. Any further distribution of this work must maintain attribution to the author(s) and the title of the work, journal citation and DOI.

candidate for addressing long-standing unsolved problems in solar physics, including coronal heating and solar wind acceleration (De Pontieu et al. 2007; McIntosh et al. 2011; Jess et al. 2012).

The detection of Alfvénic waves in the chromospheric threadlike structures has been achieved using two methods: the imaging method and the spectroscopic method. Both methods involve investigating the swaying motion of the threadlike structures and examining whether there are components oscillating horizontally with respect to the magnetic field lines. The imaging method measures the transverse displacement of the threadlike structures in the plane of the sky, which is perpendicular to the line of sight (LOS). Most studies of Alfvénic waves have primarily utilized the imaging method (e.g., Jess et al. 2012; Jafarzadeh et al. 2017; Mooroogen et al. 2017). This method has been widely employed to study Alfvénic waves in diverse regions of the chromosphere (for reviews, see Tsiropoula et al. 2012). On the other hand, the spectroscopic method has been used in only a limited number of studies to date. The spectroscopic method measures the Doppler shifts induced by threadlike structures oscillating in the LOS direction. The first spectroscopic detection of Alfvénic waves was carried out in sunspot regions and revealed the prevalence of Alfvénic waves in superpenumbral fibrils (Chae et al. 2021b). Subsequently, Chae et al. (2022) detected numerous Alfvénic wave packets in superpenumbral fibrils and presented statistics of their period, velocity amplitude, and propagation speed.

Indeed, various studies have detected Alfvénic waves in different regions, revealing diverse wave properties across these distinct regions. In particular, Kuridze et al. (2012)

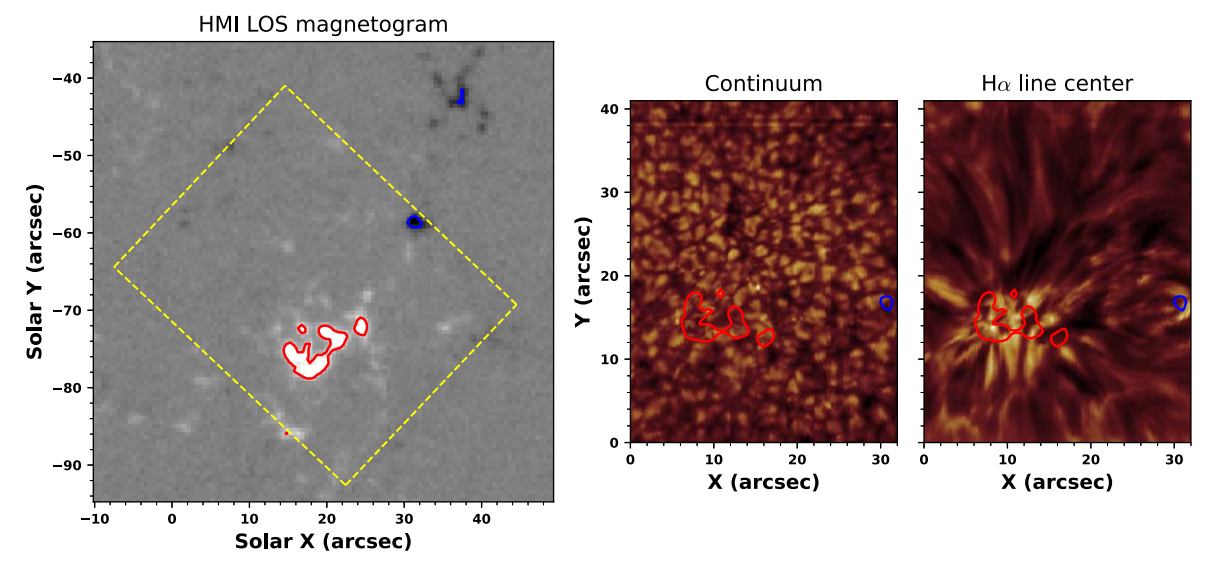


Figure 1. Left: SDO/HMI LOS magnetogram of a quiet-Sun region taken at 17:29:15 UT (t = 41 minutes) on 2020 July 30. The yellow dashed rectangle represents the FOV of the FISS. Middle: FISS H α -4 Å raster image. Right: H α line center image. The blue and red contours represent LOS magnetic field strengths of -200 and 200 G, respectively.

investigated mottles in the quiet Sun and reported the statistical properties of these waves. They found that the periods ranged from 70 to 280 s, the velocity amplitudes ranged from 3 to and the propagation speeds ranged from 40 to 110 km s⁻¹. Similarly, Jafarzadeh et al. (2017) studied slender Ca II H fibrils in an active region, including small pores and plages, and presented the wave properties observed in the region. The periods, velocity amplitudes, and propagation speeds are found to be within the ranges of 16–199 s, 1.0–4.8 km s⁻¹, and 1–70 km s⁻¹, respectively. These findings in previous studies indicate that Alfvénic waves in different regions exhibit different wave properties, providing valuable clues to their origin and underlying physical processes. In addition, the wave properties measured in diverse regions can be utilized as diagnostic tools for studying the plasma properties, such as magnetic field strength and density, within the threadlike structures in the chromosphere.

In this paper, we report the spectroscopic detection of Alfvénic waves in fibrils of the quiet Sun using high spatial and spectral resolution data. Our main objective is to analyze the wave properties of Alfvénic waves, specifically within quiet-Sun fibrils. We provide the statistical properties of these waves and compare them with previous studies. Our findings reveal that the detected waves can be classified into three distinct groups based on their periods, namely, 3, 5, and 10 minute waves, suggesting a possible relationship between their generation mechanisms. The successful detection of previously undiscovered 5 and 10 minute waves, which are characterized by relatively small velocity amplitudes, can be attributed to our use of the spectroscopic method.

2. Observations and Data Analysis

We analyzed the H α imaging spectral data obtained by the Fast Imaging Solar Spectrograph (FISS; Chae et al. 2013) of the 1.6 m Goode Solar Telescope (Cao et al. 2010) at the Big Bear Solar Observatory on 2020 July 30. The FISS, which is a dual-band echelle spectrograph, records simultaneous H α and Ca II 8542 Å spectrograms with two cameras. The images can be produced in a raster mode by scanning a slit over the field of

view (FOV) with a step size of 0."16. The size of the FOV is $24'' \times 40''$, which is equivalent to a 150-step raster mode, and the scanning is done at a cadence of 25 s. The spatial sampling along the slit is 0.116, and the spectral sampling is 0.019 Å in the H α band and 0.026 Å in the Ca II band. The wavelength ranges are 9.7 Å for the H α band and 13.1 Å for the Ca II band. With this instrument, we observed a quiet-Sun region (X = 20'', Y = -72'') from 16:48:12 to 18:10:57 UT (hereafter, the time 16:48:12 UT is referred to as t = 0). The observations were carried out with the aid of the 308 subaperture adaptive optics (Cao et al. 2010). Besides, we used the LOS magnetogram data taken with the Solar Dynamics Observatory (SDO) HMI to figure out the magnetic environment of the observed region. Figure 1 shows that the observed region includes some smallscale magnetic field concentrations that comprise a portion of the network features. The network region forms a boundary of supergranular cells with magnetic elements of mixed polarities. Since the magnetic field strength of the network region is not as strong as that of sunspots and pores, the network features are not visible in the continuum image. However, in the $H\alpha$ line center image, short bright fibrils are found at the same location as the network magnetic elements, and a large number of dark fibrils emanate from the network region.

We applied the multilayer spectral inversion (MLSI) technique (Chae et al. 2020, 2021a) to our data in order to derive the physical parameters of the chromospheric plasmas. The inversion process takes into account a radiative transfer model comprising three layers. In this model, the lowest layer corresponds to the photosphere, while the two upper layers are associated with the chromosphere. Within the photospheric layer, the absorption profile remains constant with height. In contrast, within the chromospheric layer, the absorption profile changes with optical depth in each individual layer. The threelayer model is characterized by a total of 15 parameters, with 10 of them determined through constrained least-squares fitting. The inversion process, however, demands a significant amount of computing time. For instance, processing the $H\alpha$ data used in this study takes approximately 11 days. In response to this computational challenge, Lee et al. (2022) developed a fast MLSI method based on deep learning. This

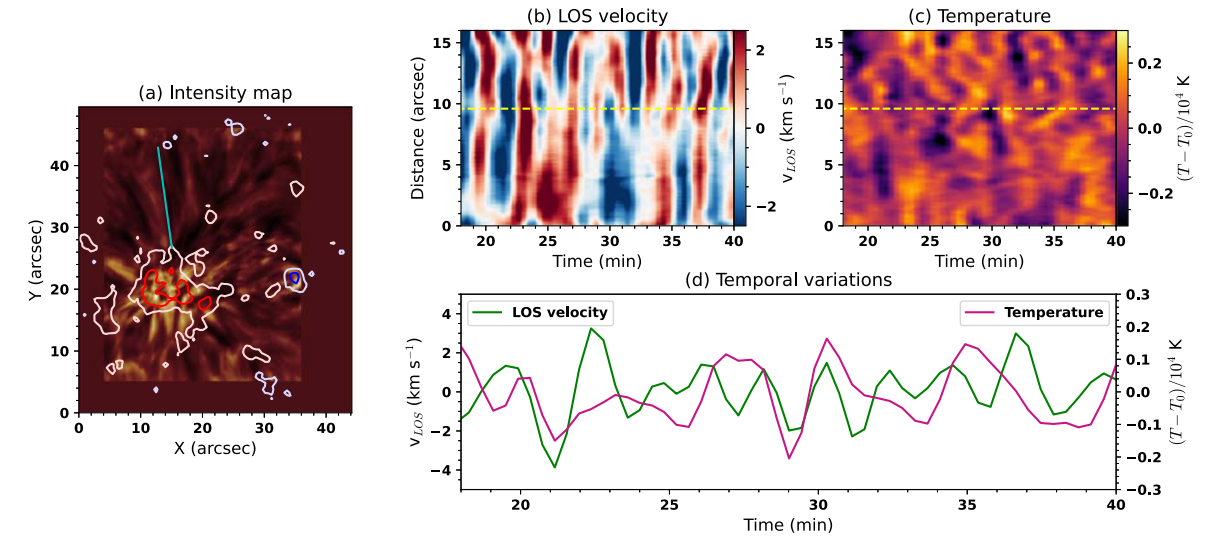


Figure 2. (a) A map of chromospheric intensity obtained from MLSI. The cyan line marks the selected fibril for detailed analysis in (b), (c), and (d). The contours in blue indicate the LOS magnetic field strengths of -30 and -200 G, and the contours in red indicate magnetic field strengths of 30 and 200 G. The darker shades of each color represent stronger magnetic field strength. (b) and (c) Time–distance plots of the LOS velocity and temperature constructed along the cyan line in the chromospheric intensity map (panel (a)). The velocity and temperature signals have been bandpass-filtered with periods from 1.5 to 22 minutes. (d) Temporal variations of the LOS velocity (green) and temperature (violet) at the position marked with a yellow dashed line in the time–distance plots (panels (b) and (c)).

approach successfully reproduced physical parameters with high accuracy while reducing computing time by approximately 250 times compared to the direct application of MLSI (Lee et al. 2022). According to Lee et al. (2022), correlation coefficients between the physical parameters obtained from the original MLSI and the fast MLSI were found to be close to 1 for most of the physical parameters. In our analysis, we used the inversion data obtained from the fast MLSI, and the full inversion results of these data can be found in Lee et al. (2022). From the inversion, we obtained maps of various physical parameters in the three layers, including source functions, Doppler velocities, Doppler widths, and so on. Among the parameters acquired from the inversion, we specifically utilized the Doppler velocity at the top of the upper chromosphere to detect Alfvénic waves in quiet-Sun fibrils. In addition, we constructed intensity maps at the H α center by combining source functions from the two chromospheric layers. These intensity maps are very useful for identifying fibrils because they are not affected by Doppler shifts, unlike monochromatic images obtained at a specific wavelength of the H α line profile.

The detection of Alfvénic waves in our study is based on the method originally introduced by Chae et al. (2022). Here, we present a concise overview of the method. The detection process comprises two main components: bandpass filtering and cross-correlation analysis. Initially, the LOS velocity maps obtained from the MLSI show a mixture of various velocity signals, each with different periods. The LOS motions of the fibrils can overlap, implying that Alfvénic waves of different periods may coexist at a single position within the fibril, which is comprised of multiple threads. Additionally, the prevalence of downflows at the footpoints of the fibrils can obscure the LOS motions of the fibrils themselves. Therefore, to accurately detect Alfvénic waves within the fibrils, we employed a decomposition technique using bandpass filtering into three distinct period bands. The decomposition process was carried out across period bands of 1.5-4, 4-8, and 8-30 minutes. To ensure the detection of waves with periods near the band boundaries, we also examined different sets of period bands. After applying the bandpass filtering to all data points within

the LOS velocity maps, we obtained a time series of bandpassfiltered LOS velocities, each filtered to a distinct period band. For the subsequent cross-correlation analysis, we manually selected two adjacent points along the same fibril at a specific time. Fibrils can be identified either in the intensity maps as intensity threads or in the bandpass-filtered velocity maps as velocity stripes. Then, we analyzed the bandpass-filtered velocity signals obtained from these two points. We first verified that the velocity signals do not show any correlation with intensity or temperature signals to exclude compressible waves. Then, we calculated the cross-correlations between the two velocity signals. Along the same fibril, we repeatedly changed the distance between two points, ensuring that the cross-correlation exceeded 0.9. Ultimately, we chose the two points having the maximum distance while still maintaining a cross-correlation value above 0.9. Typically, these two points are spaced about 1."6 apart. For wave packets with crosscorrelations exceeding 0.9 and velocity amplitudes over 0.25 km s⁻¹, we classified them as Alfvénic wave packets. We also determined the propagation speed by measuring the distance between the two adjacent points along the fibrils and calculating the time lag in the velocity signals between these points. In this analysis, we considered additional time shifts that arise from the data acquisition process, i.e., the scanning of the FOV by the slit. Note that the estimation of the propagation speeds was carried out on the image plane.

3. Results

We found that Alfvénic waves are also pervasive in the fibrils of a quiet region, as previously shown in sunspot regions through the spectroscopic method (Chae et al. 2021b, 2022). The left panel of Figure 2 shows the chromospheric intensity map of the network region obtained from the MLSI of the $H\alpha$ data. Note that the chromospheric intensity map shows a high similarity to the $H\alpha$ line center image in Figure 1. The network region is surrounded by a large number of dark and bright fibrils. Mostly, dark fibrils extend further into the internetwork region, while short bright fibrils are distributed around the

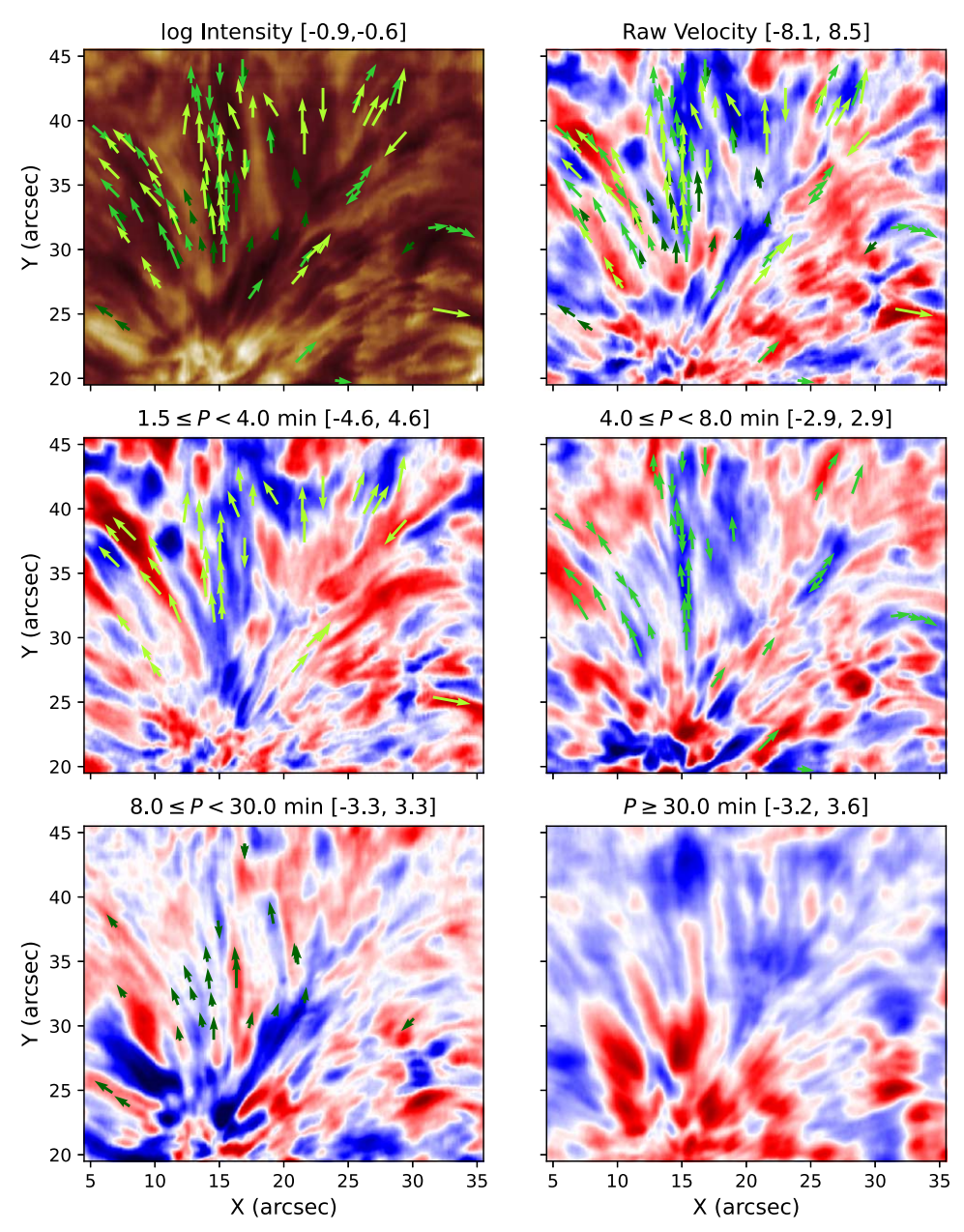


Figure 3. The top panels display the H α intensity and LOS velocity maps acquired from the MLSI. The following panels show the velocity maps filtered by different period bands, i.e., 3, 5, 10, and longer than 30 minutes periods. During the 20 minute time interval, 131 wave packets were detected. The arrows indicate detected wave packets, with their centers positioned at the midpoint between two selected points used for cross-correlation analysis. The direction of the arrows indicates the wave propagation direction. The length of the arrows represents the propagation speed, which is proportional to $c^{1/3}$. The propagation speeds range from 21 to 405 km s⁻¹. The colors of the arrows indicate the wave packets belonging to different period bands. The light green arrows represent 3 minute waves, medium green arrows represent 5 minute waves, and dark green arrows represent 10 minute waves.

network region. Among the dark fibrils, one stable fibril was selected as an example. The fibril initially appeared at t=18 minutes, repeatedly appearing and disappearing intermittently. However, it completely vanished at t=39 minutes. Thus, within that time interval, we constructed time–distance plots of the LOS velocity and temperature along the cyan line in Figure 2(a). In general, fibrils are highly inclined to the horizontal direction, so the observed LOS velocity oscillations in the time–distance plot represent transverse MHD waves propagating along the fibrils. The time–distance plot of the LOS velocity reveals the presence of numerous velocity oscillation patterns with various periods and durations (see Figure 2(b)). Moreover, the different slope of the velocity stripes indicates that some wave packets propagate faster out of the network

elements, while others exhibit slower propagation. It implies that transverse waves with different propagation speeds can coexist within the same fibril. It has been reported that a similar phenomenon is also observed in the fibrils of sunspot regions, and it has been interpreted as an effect of multiple fibrils located in the LOS overlapping with each other, rather than coexisting in one actual location (Chae et al. 2022). In the time–distance plot of temperature, however, no clear oscillation patterns associated with the velocity oscillations were observed (see Figure 2(c)). We also examined the temporal variations of the velocity and temperature acquired at one position in the cut (yellow dashed line in the time–distance plots of Figures 2(b) and (c)). It appears that the period of the LOS velocity oscillations is even shorter than that of the temperature

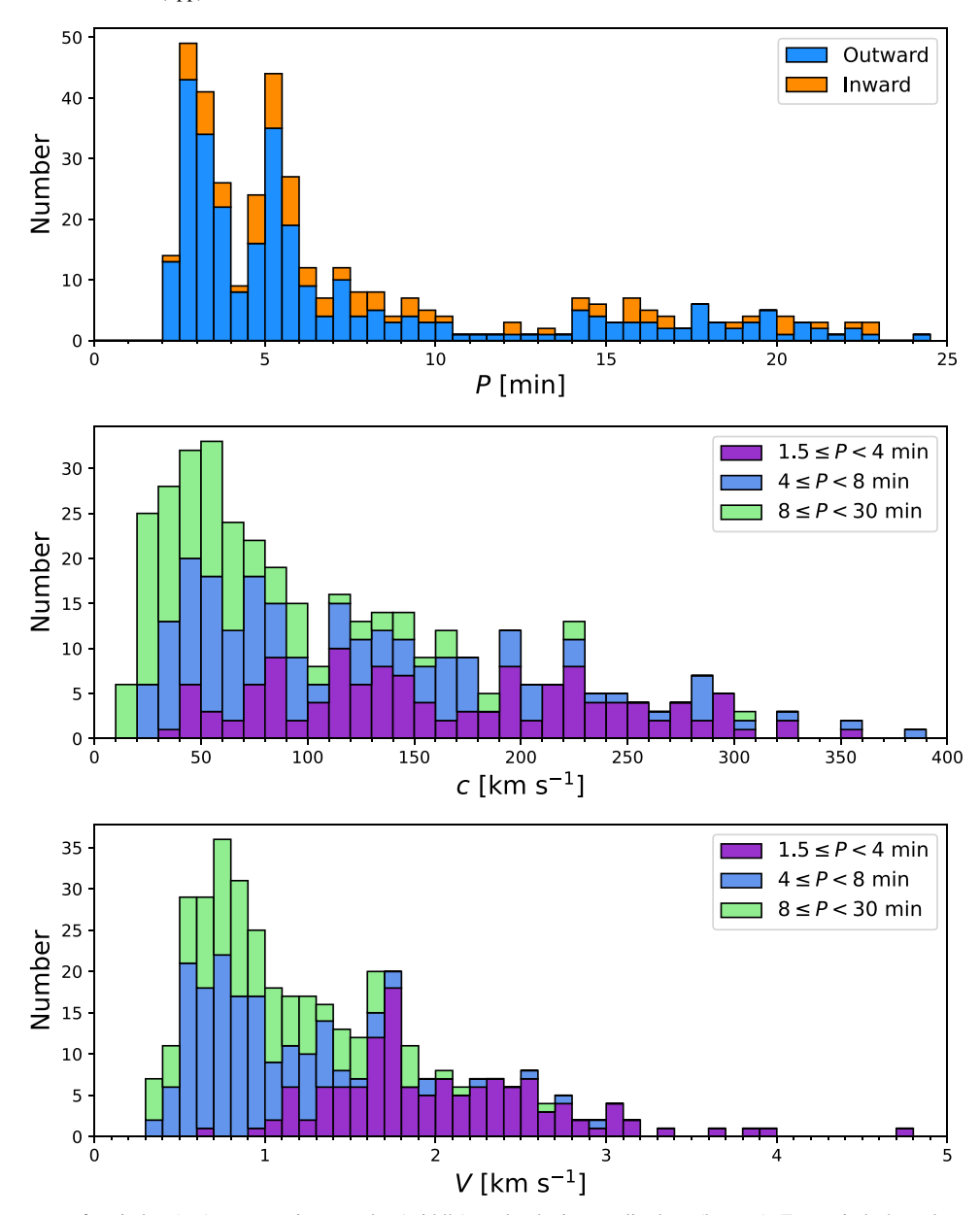


Figure 4. Stacked histograms of period P (top), propagation speed c (middle), and velocity amplitude V (bottom). For period, the values are divided into outward waves and inward waves. For propagation speed and velocity amplitude, the values are grouped into three bands based on their periods: 3, 5, and 10 minute bands.

oscillations. Furthermore, the cross-correlation coefficient between the time series of the velocity and temperature is 0.2, which confirms that velocity oscillations are not correlated with temperature oscillations. Therefore, we suggest that the LOS velocity oscillations observed in the fibril indicate the presence of Alfvénic waves, which are transverse MHD waves that are either weakly compressible or incompressible.

Figure 3 illustrates the spatial distribution of the observed Alfvénic wave packets during a specific 20 minute time interval centered at t=41 minutes. The majority of the wave packets are found in the upper part of the network region, where the fibrils are well developed. The 3 minute band includes periods ranging from 1.5 to 4 minutes, the 5 minute band includes periods from 4 to 8 minutes, and the 10 minute band includes periods from 8 to 30 minutes. Interestingly, the waves in the 10 minute band are mainly confined to near the footpoints of the fibrils, while the waves in the 3 and 5 minute bands tend to extend further out. This tendency is in agreement with previous

studies of Alfvénic waves detected in superpenumbral regions (Morton et al. 2021; Chae et al. 2022). However, it does not necessarily mean that the locations where the shorter and longer periods of waves appear are spatially separated. Rather, wave packets in different bands often overlap.

In each bandpass-filtered LOS velocity map in Figure 3, most of the wave packets are distributed along the fibrils. Moreover, the wave packets in the same period band tend to appear along a single fibril, indicating that each fibril or flux tube carries waves in a specific period band. This is particularly evident in the velocity map of the 5 minute band at around (x, y) = (15'', 30''-43'').

As it has been confirmed that Alfvénic waves are abundant in the quiet-Sun fibrils, we closely identified each wave packet and investigated its properties statistically. We found a total of 385 Alfvénic wave packets and inspected their period, velocity amplitude, and propagation speed. Figure 4 shows the number distribution of each wave property. In the case of a period, the

Table 1
Mean Values and Standard Deviations of the Physical Parameters of the Waves

Parameters	3 Minute Waves	5 Minute Waves	10 Minute Waves	All Waves
Period (minutes)	3.1 ± 0.44	5.7 ± 0.92	15 ± 4.5	7.5 ± 5.6
Velocity amplitude (km s ⁻¹)	2.03 ± 0.65	0.93 ± 0.44	1.01 ± 0.44	1.33 ± 0.74
Propagation speed (km s ⁻¹)	168 ± 79	114 ± 82	67 ± 51	123 ± 90
Outward propagation fraction (%)	86	73	69	77

wave packets are divided into three groups, i.e., 3, 5, and 10 minute periods (top panel of Figure 4). The boundary between the shorter periods (<10 minutes) and longer periods (>10 minutes) is obvious, as can be seen from the existence of a minimum between the two groups. Likewise, the boundary between the 3 and 5 minute periods is also well defined, with a minimum value at around 4 minutes. Notably, there are two prominent peaks at periods of 3 and 5.5 minutes. The overall distribution of the shorter periods (<10 minutes) exhibits a broad-tailed distribution, which is noticeably different from that of the longer periods (>10 minutes). The longer-period waves have a much broader distribution without a clear peak. It suggests a potential physical implication associated with a similar generation mechanism for the 3 and 5 minute waves, which is distinct from that of the 10 minute waves. The propagation direction of the wave packets is mainly outward, regardless of the period. We examined the distribution of wave propagation speeds for each period group. The middle panel of Figure 4 shows that shorter-period waves have higher propagation speeds. The correlation coefficient between $\log c$ and $\log P$ is -0.57, indicating a negative correlation. We investigated the distribution of velocity amplitudes within each period group (bottom panel of Figure 4). It was found that the wave packets in the 3 minute band have much larger velocity amplitudes compared to those in the other bands. Wave packets within the 5 and 10 minute bands have smaller velocity amplitudes, but there is no obvious trend related to velocity amplitudes between these two bands.

We examined the mean values and standard deviations of the wave properties, which are summarized in Table 1. Since we have confirmed that there are three groups in the wave periods, all parameters are given for each group. Additionally, the values for all of the wave packets are also presented. Out of a total of 385 wave packets, 130 are in the 3 minute band, 143 are in the 5 minute band, and 112 are in the 10 minute band. For each of the three bands, the mean period values are 3.1, 5.7, and 15 minutes for the 3, 5, and 10 minute bands, respectively. Similarly, the mean velocity amplitudes for the respective bands are 2.03, 0.93, and 1.01 km s⁻¹, and the mean propagation speeds are 168, 114, and 67 km s⁻¹. We also examined the propagation direction of the waves for each period band and found that 86% of the wave packets in the 3 minute band, 73% in the 5 minute band, and 69% in the 10 minute band propagate outward from the fibrils.

For all wave packets, the mean values of the period, velocity amplitude, and propagation speed are 7.5 minutes, 1.33 km s⁻¹, and 123 km s⁻¹, respectively. When considering all of the wave packets, 77% of them propagate outward. The statistics can be compared with those of fibrils in sunspot regions. Using the same method, Chae et al. (2022) found that the mean values of the period, velocity amplitude, and propagation speed are 6.5 minutes, 0.6 km s⁻¹, and 100 km s⁻¹, respectively. The mean period and propagation speed values are similar in both regions, but the velocity amplitude is twice as large in the quiet

Sun. Moreover, in sunspot regions, most waves in the 3 minute band propagate outward, but only half of the waves in the 10 minute band propagate outward, as opposed to the majority of waves in the 10 minute band propagating outward in the quiet-Sun region.

By utilizing the wave properties obtained above, we roughly estimated the wave energy flux. The wave energy flux is given by the expression

$$F = \frac{1}{2}\rho V^2 c,\tag{1}$$

where ρ is the mass density, V is the velocity amplitude, and c is the propagation speed. Theoretically, Alfvénic waves propagate with the local Alfvén speed, which is given by the expression

$$c = \frac{B}{\sqrt{4\pi\rho}},\tag{2}$$

where B is the magnetic field strength. Instead of determining the mass density values within the fibril, Equation (1) can be rearranged using Equation (2) to express the wave energy flux in terms of velocity amplitude, propagation speed, and magnetic field strength. In our analysis, we utilized estimated values of the velocity amplitude and propagation speed for 385 Alfvénic wave packets. For the magnetic field strength, we adopted a value of \sim 50 G, which corresponds to the value for network elements at the chromospheric height (Centeno et al. 2010; Ishikawa et al. 2021). Based on these values, the estimated mean wave energy flux is 1.4×10^5 erg s⁻¹ cm⁻². However, this value is significantly smaller than the energy flux required for the chromospheric heating in the quiet Sun, which is known to be 4×10^6 erg s⁻¹ cm⁻² (Withbroe & Noyes 1977). Furthermore, this value is also smaller than the wave energy flux estimated in sunspot regions, which corresponds to $3.7 \times 10^5 \text{ erg s}^{-1} \text{ cm}^{-2}$ (Chae et al. 2022).

4. Summary and Discussion

For the first time, we have reported the spectroscopic detection of Alfvénic waves in the quiet-Sun fibrils. The transverse motion of elongated threadlike structures, such as fibrils, indicates the presence of transverse MHD waves in the chromosphere. On-disk fibrils represent highly inclined magnetic field lines in the chromosphere, and their LOS oscillations in spectral data reveal the existence of transverse MHD waves. Using the $H\alpha$ spectral data, we detected 385 Alfvénic wave packets in the quiet Sun and investigated their wave properties, including period, velocity amplitude, propagation speed, and propagation direction. Based on their periods, the waves were classified into three groups: 3, 5, and 10 minute waves. We presented statistics on the wave properties for each period group (See Table 1). The mean

values of the period, velocity amplitude, and propagation speed for all of the wave packets are 7.5 minutes, 1.33 km s⁻¹, and 123 km s⁻¹, respectively. Additionally, we found that 77% of the waves propagate outward. Indeed, the successful detection of additional 5 and 10 minute waves, characterized by small velocity amplitudes and previously undetected in earlier studies, can be attributed to our implementation of the spectroscopic method, which enables the measurement of waves with such small velocity amplitudes.

Our measurement of wave properties using the spectroscopic method allows for comparison with values reported in previous studies that used the imaging method. There are several imaging-based transverse MHD wave studies associated with the chromospheric elongated threadlike structures, such as fibrils, mottles, and spicules, in the quiet Sun (Jafarzadeh et al. 2017, and references therein). Specifically, Mooroogen et al. (2017) provided the wave properties of internetwork chromospheric fibrils. The mean values of the period, velocity amplitude, and propagation speed are 128 s, 4.22 km s⁻¹, and 446 km s⁻¹, respectively. Kuridze et al. (2012) investigated long-lived quiet-Sun mottles in the H α image and found that the wave periods range from 70 to 280 s, with a strong peak at 165 s. Furthermore, the velocity amplitudes range from 3 to 18 km s⁻¹ with a median value of 8 km s⁻¹, and propagation speeds range from 40 to 110 km s⁻¹.

One notable difference in our study is the identification of three groups in the wave period, which has not been reported in quiet-Sun fibril studies using the imaging detection method. We found three distinct groups based on wave period, and the mean period of each group is 3.1, 5.7, and 15 minutes for the 3, 5, and 10 minute bands, respectively. The 3 minute band in our study displays a period range of 2.2-3.9 minutes, which is in agreement with the values previously reported in studies that utilized the imaging detection method (Kuridze et al. 2012; Mooroogen et al. 2017). However, waves with periods of 5 and 10 minutes have not been reported in previous quiet-Sun fibril studies using the imaging method. We conjecture that this may be related to the smaller velocity amplitudes of the 5 and 10 minute waves compared to the 3 minute waves, as observed in our study. Specifically, we found that the mean velocity amplitude of the 3 minute waves is $2.03~{\rm km\,s}^{-1}$, while those of the 5 and 10 minute waves are 0.93 and 1.01 km s⁻¹, respectively. Without bandpass filtering, the oscillations of all periods are mixed together, and only the stronger oscillations are distinguishable. Therefore, the transverse motions of the longer-period waves may not be as conspicuous due to their smaller amplitudes and may not have been detected in previous imaging-based studies. Moreover, it is important to note that waves with small velocity amplitudes tend to exhibit small transverse displacements in imaging data. Consequently, the detection of small-amplitude waves using the imaging method is highly reliant on the resolution of the image data. On the other hand, the spectroscopic method, which directly measures the LOS velocity within the fibrils, is not affected by the resolution of the image data. This allows for the detection of the longer-period waves with smaller velocity amplitudes that might have been missed in imaging-based studies.

The velocity amplitudes measured in our study are smaller than those reported in previous studies. Considering only waves in the 3 minute band, the mean velocity amplitude measured in our study is 2.03 km s⁻¹, which is less than half the value reported in imaging-based studies (Kuridze et al.

2012; Mooroogen et al. 2017). This discrepancy may be explained by the effect of gravity, which can hinder LOS oscillations more strongly than horizontally directed transverse oscillations. As a result, the velocity amplitude may be smaller in the spectroscopic method, which measures in the LOS direction, compared to the imaging method, which measures in the horizontal direction. However, despite considering the possible influence of gravity, the velocity amplitudes measured in this study are still considerably smaller compared to those reported in previous studies suggesting Alfvénic waves as a potential energy source for coronal heating and solar wind acceleration (De Pontieu et al. 2007; McIntosh et al. 2011; Jess et al. 2012). In particular, Jess et al. (2012) reported that velocity amplitudes of transverse waves in type I spicules often exceed $15 \,\mathrm{km \, s^{-1}}$. It is worth noting that the detection of transverse waves using the imaging method can be selective, as it often focuses on capturing the most prominent motions with large amplitudes in order to effectively resolve the transverse motions of threadlike structures. Nevertheless, the question still remains as to why waves with large velocity amplitudes have not been detected using the spectroscopic method. Even the largest amplitudes obtained through the spectroscopic method are significantly smaller than those detected using the imaging method. Therefore, it is challenging to confirm whether the Alfvénic waves detected by the spectroscopic method are of the same kind as those detected by the imaging method or not, and if so, how the two different methods can be combined for a more comprehensive view. More important may be to determine the velocity amplitudes of the Alfvénic waves that are typical or representative of quiet regions. We expect that a follow-up study using the FISS, which is capable of obtaining both images and spectra simultaneously, will provide valuable insights into the nature of Alfvénic waves. By detecting these waves in both images and spectra, we can better understand their properties and generation and how they relate to the magnetic environment of the structures they propagate through.

The mean propagation speed of the 3 minute waves in our study is 168 km s⁻¹ with a range of 32–405 km s⁻¹, which partially overlaps with those reported in the imaging-based studies (Kuridze et al. 2012; Mooroogen et al. 2017). It is important to note that the ranges of mean propagation speed in each study are considerably wide. However, as shown in Equation (2), the propagation speed of Alfvénic waves is highly dependent on the local magnetic field strength and mass density of the magnetic flux tube, which can vary significantly from one location to another. Therefore, it is not surprising that there are significant discrepancies in the reported mean propagation speeds between different studies, as well as large standard deviations.

Interestingly, we found that the Alfvénic wave properties in our study exhibit strong similarities to those observed in sunspot regions using the spectroscopic method (Chae et al. 2021b, 2022). In sunspot regions, the mean values of the period, velocity amplitude, and propagation speed for all of the wave packets are 6.5 minutes, 0.6 km s⁻¹, and 100 km s⁻¹, respectively (Chae et al. 2022), which are mostly consistent with our findings in the quiet Sun. However, we noticed a slight difference in the velocity amplitude compared to the sunspot regions, which was about a factor of 2 larger. This difference may be attributed to the distinct magnetic environments of the two regions, as the magnetic field strength is typically weaker in the network of the quiet Sun relative to

the sunspot regions. The expression for the wave energy density is given by

$$U = \frac{1}{2}\rho V^2 = \frac{B^2}{8\pi} \left(\frac{V}{c}\right)^2.$$
 (3)

In a small sunspot region, Chae et al. (2022) reported a mean wave energy density carried by Alfvénic waves of 3.9 × 10^{-2} erg cm⁻³. In this study, we calculated the mean wave energy density in the quiet-Sun region to be 1.6×10^{-2} erg cm⁻³. This yields a wave energy density ratio of 2.4 between the two regions. By utilizing the energy density ratio and Equation (3), we identified an inverse relationship between magnetic field strengths and velocity amplitudes with a proportional factor of 0.6. This predicts that the quiet-Sun region, with its weaker magnetic field, would exhibit a larger velocity amplitude than the sunspot regions. Specifically, the velocity amplitude is expected to be doubled in the quiet Sun if the magnetic field strength in the sunspot region is three times greater than in the quiet-Sun region. Given a magnetic field strength of 50 G in the quiet Sun, estimating 150 G in the sunspot chromosphere is indeed a reasonable estimate (Chae et al. 2022). This finding has significant implications for helioseismology, as it provides a way to estimate physical properties such as magnetic field strength and mass density in different regions of the Sun.

Another similarity to the waves detected in sunspot regions is that the detected waves in our study are also classified into groups based on their period. Chae et al. (2022) reported the existence of two groups of Alfvénic waves in sunspot regions, namely, 3 and 10 minute waves. Similarly, in our study, we have identified two main groups in the number distribution of periods, as shown in Figure 4, with a clear minimum between the two groups at around 10 minutes. The waves are initially categorized into two groups: shorter periods (<10 minutes) and longer periods (>10 minutes). However, an additional peak at 5 minutes was also found, which led us to classify the waves into three distinct groups, i.e., 3, 5, and 10 minute waves. Despite this slight difference, the characteristics of the waves detected in both regions are very similar. These similarities are likely a result of the interaction between acoustic waves in the photosphere and the magnetic fields as they propagate upward into the chromosphere, occurring in both the quiet-Sun (Kontogiannis et al. 2014) and sunspot regions (Krishna Prasad et al. 2016).

We suggest that the Alfvénic waves identified in our study may have the same origin as those reported in sunspot regions by Chae et al. (2022). According to their findings, 3 minute waves arise from slow-to-Alfvénic mode conversion, while 10 minute waves arise from convective motions in the photosphere. Although the details are different, this is in line with numerous studies that have proposed wave mode conversions (Raboonik & Cally 2019; Cally 2022) and convective motions (Spruit 1981; Choudhuri et al. 1993) as potential sources of Alfvénic waves. Regarding the 5 minute waves we detected, we propose that they likely originate from the same mechanism as the 3 minute waves. In network regions, slow waves with longer periods on the order of 5 minutes are predominant (e.g., Lites et al. 1993). This is because the large inclination angle of the magnetic field lines comprising the fibrils allows the longerperiod slow waves to propagate upward (De Pontieu et al. 2004; Jefferies et al. 2006; Kontogiannis et al. 2010). At some height, the upward-propagating 5 minute waves are converted into

Alfvénic waves of the same period. Therefore, the 5 minute period Alfvénic waves may also arise from the slow-to-Alfvénic mode conversion, similar to the 3 minute waves. While slow-to-Alfvénic mode conversion and convective motions are believed to be the main mechanisms for generating Alfvénic waves in the solar atmosphere, there could be other mechanisms as well, such as magnetic reconnections (Pietarila et al. 2011). In the case of inward-propagating waves, we propose several possible explanations. These waves may originate from the other footpoints of the fibrils, experience reflection at the transition region due to variations in the Alfvén speed with height, or have their source located in the transition region and propagate downward (Chae & Lee 2023). Further studies are necessary to fully understand the origin and propagation of the Alfvénic waves in various regions of the Sun.

Acknowledgments

We thank the referee for careful manuscript reading, constructive comments, and insightful suggestions. This research was supported by the Korea Astronomy and Space Science Institute under the R&D program (project No. 2023-1-850-07) supervised by the Ministry of Science and ICT. J.C. was supported by the National Research Foundation of Korea (RS-2023-00208117). K.-S.L. was supported by the National Research Foundation of Korea (NRF-2021R1A2C1010881), funded by the Korean Ministry of Science and ICT. We gratefully acknowledge the use of data from the Goode Solar Telescope (GST) of the Big Bear Solar Observatory (BBSO). BBSO operation is supported by US NSF grants AGS-2309939 and AGS-1821294 and the New Jersey Institute of Technology. GST operation is partly supported by the Korea Astronomy and Space Science Institute and the Seoul National University.

ORCID iDs

Hannah Kwak https://orcid.org/0000-0001-8619-9345
Jongchul Chae https://orcid.org/0000-0002-7073-868X
Eun-Kyung Lim https://orcid.org/0000-0002-7358-9827
Kyoung-Sun Lee https://orcid.org/0000-0002-4329-9546
Donguk Song https://orcid.org/0000-0003-3034-8406
Heesu Yang https://orcid.org/0000-0001-5455-2546

References

```
Cally, P. S. 2022, MNRAS, 510, 1093
Cao, W., Gorceix, N., Coulter, R., et al. 2010, AN, 331, 636
Centeno, R., Trujillo Bueno, J., & Asensio Ramos, A. 2010, ApJ, 708, 1579
Chae, J., Cho, K., Kang, J., et al. 2021a, JKAS, 54, 139
Chae, J., Cho, K., Lim, E.-K., & Kang, J. 2022, ApJ, 933, 108
Chae, J., Cho, K., Nakariakov, V. M., Cho, K.-S., & Kwon, R.-Y. 2021b,
   ApJL, 914, L16
Chae, J., & Lee, K.-S. 2023, ApJ, 954, 45
Chae, J., Madjarska, M. S., Kwak, H., & Cho, K. 2020, A&A, 640, A45
Chae, J., Park, H.-M., Ahn, K., et al. 2013, SoPh, 288, 1
Choudhuri, A. R., Auffret, H., & Priest, E. R. 1993, SoPh, 143, 49
De Pontieu, B., Erdélyi, R., & James, S. P. 2004, Natur, 430, 536
De Pontieu, B., McIntosh, S. W., Carlsson, M., et al. 2007, Sci, 318, 1574
Ishikawa, R., Trujillo Bueno, J., del Pino Alemán, T., et al. 2021, SciA, 7,
Jafarzadeh, S., Solanki, S. K., Gafeira, R., et al. 2017, ApJS, 229, 9
Jefferies, S. M., McIntosh, S. W., Armstrong, J. D., et al. 2006, ApJL,
  648, L151
Jess, D. B., Morton, R. J., Verth, G., et al. 2015, SSRv, 190, 103
Jess, D. B., Pascoe, D. J., Christian, D. J., et al. 2012, ApJL, 744, L5
Kontogiannis, I., Tsiropoula, G., & Tziotziou, K. 2014, Â&A, 567, A62
```

Kontogiannis, I., Tsiropoula, G., Tziotziou, K., & Georgoulis, M. K. 2010,

A&A, 524, A12

Krishna Prasad, S., Jess, D. B., Jain, R., & Keys, P. H. 2016, ApJ, 823, 45 Kuridze, D., Morton, R. J., Erdélyi, R., et al. 2012, ApJ, 750, 51 Kuridze, D., Verth, G., Mathioudakis, M., et al. 2013, ApJ, 779, 82 Lee, K.-S., Chae, J., Park, E., et al. 2022, ApJ, 940, 147 Leenaarts, J., Carlsson, M., & Rouppe van der Voort, L. 2012, ApJ, 749, 136 Lites, B. W., Rutten, R. J., & Kalkofen, W. 1993, ApJ, 414, 345 McIntosh, S. W., de Pontieu, B., Carlsson, M., et al. 2011, Natur, 475, 477 Mooroogen, K., Morton, R. J., & Henriques, V. 2017, A&A, 607, A46

Morton, R. J., Mooroogen, K., & Henriques, V. M. J. 2021, RSPTA, 379, 20200183
Pietarila, A., Aznar Cuadrado, R., Hirzberger, J., & Solanki, S. K. 2011, ApJ, 739, 92
Raboonik, A., & Cally, P. S. 2019, SoPh, 294, 147
Spruit, H. C. 1981, A&A, 98, 155
Tsiropoula, G., Tziotziou, K., Kontogiannis, I., et al. 2012, SSRv, 169, 181

Withbroe, G. L., & Noyes, R. W. 1977, ARA&A, 15, 363